Photochemical & Photobiological Sciences (2021) 20:303–313
https://doi.org/10.1007/s43630-021-00019-9

ORIGINAL PAPERS

pH-controlled mechanism of photocatalytic RhB degradation over g-C_3N_4 under sunlight irradiation

Weina Shi[1] · Wen-Xue Fang[2,3] · Ji-Chao Wang[3,4] · Xiu Qiao[3] · Beibei Wang[4] · Xiaowei Guo[1]

Received: 17 December 2020 / Accepted: 2 February 2021 / Published online: 20 February 2021

Abstract

Photocatalysis of dye degradation is one of green and cheap technologies for solving environmental pollution. Whereas it is rarely concerned that the degradation process varied with the change of solution condition, this work studied the influence of hydrion in the solution on the photodegradation process of Rhodamine B (RhB) over g-C_3N_4. The photocatalytic activity of RhB degradation was enhanced gradually with increased hydrion content in the system. The efficiency for RhB degradation over g-C_3N_4 in weak acidic system with interference of multiple metal-ions still reached near 95% after 30 min of natural sunlight irradiation. A large amount of oxidation species and the hydroxylation mineralization process were induced by increasing the hydrion concentration. Two degradation processes for deethylation of four ethyl groups and the direct chromophoric degradation were discovered and proved by multifarious intermediates in different systems using the ESR technique, LC/MS and GC/MS analysis. In addition, the photosensitization played a critical role in the RhB degradation. A feasible degradation mechanism was proposed for the RhB degradation based on the experimental results.

Keywords g-C_3N_4 · Hydrion · Photosensitization degradation · Sunlight · Oxidation species · Degradation process

1 Introduction

Photocatalytic technology over semiconductor is an ideal way to solve the energy problem and the environment issue using abundant solar energy [1]. In the past 40 years, a large number of studies were communicated for the photocatalysis of pollutant degradation, hydrogen production, water splitting and CO_2 reduction over various photocatalysts [2–6]. Up to now, the photocatalysis of pollutant degradation is one of the widely attentive researches, and various hypotheses have been suggested. According to the reported studies of photodegradtion [7–9], it is generally accepted that the electron–hole pairs in semiconductor are generated by illuminating light with enough energy, and the photogenerated carriers then react with dissolved oxygen or water molecules to emerge with reactive oxidizing species including hydroxyl radicals (•OH) and superoxide radicals ($\bullet O^{2-}$) [10]. Meanwhile, the photogenerated holes could decompose pollutants into small molecules [11]. In the degradation studies of organic dyes [12–14], it cannot be ignored that the excess negative charges inside the conduction band by the dye excitation are removed by molecular oxygen forming superoxide radicals, while the proton from the dye molecule is separated generating a double bond [15, 16]. Hence, it is concluded that pollutant molecules are not only oxidized by the photogenerated holes and reactive oxidizing radicals, but also offer electrons for catalysts to form reactive oxygen species in photodegradation process.

The degradation photocatalysis, as a multistep and complex process, was affected by diversified factors including the redox ability and transfer of the photogenerated carriers and the situation of catalytic solution [17–19]. Among them, the influence of the hydrion in catalytic solution on the surface state of photocatalysts cannot be ignored in photocatalytic degradation [20–22]. For instance, Merka. et al. [23] reported that adjusting the pH value of the solution changed the surface states of $Pb_3Nb_4O_{13}$ photocatalysts, the RhB

✉ Ji-Chao Wang
wangjichao@hist.edu.cn

1 School of Chemistry and Materials Engineering, Xinxiang University, Xinxiang 453003, China

2 Institute of Forensic Science, Xinxiang Municipal Public Security Bureau, Xinxiang 453003, China

3 School of Ecology and Environment, Zhengzhou University, Zhengzhou 450000, China

4 College of Chemistry and Chemical Engineering, Henan Institute of Science and Technology, Xinxiang 453000, China

photodegradation process and efficiency. Shun et. al. [24] proved that the degradation of RhB was greatly enhanced in the presence of acid, and the predominant reactive oxygen species of superoxide is responsible for the efficient degradation of RhB. Although the reported study has proven that the acid effect plays a positive role for photocatalysis of RhB degradation [25–27], the relation between the mechanism of RhB degradation and the hydrion in solution needs a detailed understanding. So far, two different mechanisms of RhB photodegradation are discussed, including the successive deethylation of the four ethyl groups and the direct degradation of the chromophoric system [28]. All degradation mechanisms of RhB were impacted by numerous conditions, such as the redox ability of photogenerated carriers, the hydrion concentration and the kinds and content of oxidizing species [23]. The formation of active oxidation radicals and species in solution was influenced by the energy band position of photocatalysts and hydrion concentration [29, 30]. Therefore, it is still urgently required to study the effect of the hydrion in solution on the interaction of the dye and the semiconductor and the formation of reactive oxidation species and the intermediates in RhB degradation.

The large surface area, appropriate band gap and chemical stability of the graphitic carbon nitride (g-C_3N_4) have drawn enormous attention in the photocatalysis fields [31]. Meanwhile the photodegradation performance of g-C_3N_4 was affected by the hydrion on the catalytic surface or in solution, depending on the previous reports [30, 32]. In the present work, the influence of pH value on the photocatalytic activity of RhB degradation over g-C_3N_4 catalyst was investigated. The rate of RhB degradation can be accelerated with decreasing pH values. The reactive oxidation species and intermediates in the RhB degradation process at different pH values were discovered using ESR, HPLC, LC/MS and MS measurement. We found that two decomposition processes were existed in photocatalytic RhB degradation with different acidity. The possible photocatalytic mechanism of RhB degradation over g-C_3N_4 was proposed on the basis of the experimental results.

2 Experimental

2.1 Photocatalyst preparation

All the reagents were of analytical grade and were used without further purification. The g-C_3N_4 was prepared by calcining method [33]. In the typical synthesis, 15 g urea powder was put into an alumina crucible with a cover. Then it was treated at 600 °C for 1 h with the heating rate of 10 °C/min. and the powder was collected after HNO_3 solution (0.5 mol/L) washing. Then an yellow powder was obtained at 550 °C for 1 h. Finally, the fluffy sample (g-C_3N_4) was washed by HNO_3 solution (0.1 mol/L) and ethyl alcohol and then dried at 80 °C. g-C_3N_4-B sample was obtained from urea by a one-step calcination at 550 °C for 2 h.

2.2 Characterization

X-ray diffraction (XRD) patterns were measured using an X'Pert PRO X-ray powder diffractometer (PANalytical, the Netherlands) with Cu-Kα radiation ($\lambda = 1.5418$ Å). The FT-IR spectra were recorded on a Nicolet Nexus spectrometer on samples embedded in KBr pellets. X-ray photoelectron spectroscopy (XPS) analysis was performed on a XSAM 800 X-ray photoelectron spectroscope (Kratos, UK) and the binding energy was calibrated on the reference C 1 s peak at 284.3 eV. UV–Vis diffuse reflectance spectrum (DRS) was obtained using a Cary 5000 UV–Vis spectrometer (Agilent Technologies, USA), using $BaSO_4$ as reference. The electron spin resonance (ESR) spectra were recorded at the X band using a Bruker EMX-10/12 spectrometer with a 100-kHz magnetic field modulation at a microwave power level of 19.9 mW.

2.3 Photocatalysis of RhB degradation

The photocatalytic tests of RhB degradation over g-C_3N_4 were carried out under visible-light irradiation at room temperature. For a typical photocatalytic experiment, 0.05 g of catalyst was suspended in 500 mL RhB aqueous solution (10 mg L^{-1}) with constant stirring. Prior to the irradiation, the suspensions were magnetically stirred in the dark for 1 h to ensure the adsorption equilibrium between catalyst and dye. Hydrochloric acid (HCl) and sodium hydroxide (NaOH) were used to adjust the original pH values of the system. During the irradiation, 5 mL sample was taken out and centrifuged at given intervals. The RhB concentration was detected spectrophotometry with 552 nm wavelength. The influence of the acidity on the photocatalytic activity was studied with 300 W Xe light irradiation. The sunlight-driven photocatalytic activity was measured from Jun. 8 to Aug. 2 2019 at our lab (N35°16′59″ E 113°55′43″) in Xinxiang City, Henan Province, China. The sunlight light intensity reached 62.2 ~ 90.4 mW/cm [2]. The RhB photosensitization was carried out as the above similar method using Xe lamp light. The reactive oxidation species during degradation process were determined by means of scavengers and ESR technique. The concentration of RhB and intermediates were determined by high-performance liquid chromatography (HPLC) (Agilent 1100, USA) using a C18 column (200 mm × 4.6 mm, 5 μm, Agilent, USA). The identification of intermediate was conducted by LC/MS/MS (Agilient 1290LC-6540 accurate mass Q-TOF, USA) equipped with an electrospray ionization (ESI) source. The intermediates were also detected by a Thermo DSQII Trace gas chromatography

interfaced with a Polaris Q ion trap mass spectrometer (GC/MS, Thermo Fisher Scientific, USA). The experiment process is detailed in Supplementary Material S1, S2 and S3.

3 Results and discussion

3.1 Characterization of g-C_3N_4

The XRD patterns of the investigated carbon nitride are shown in Fig. S1. All diffraction peaks of the as-prepared g-C_3N_4 sample were indexed as the phase of g-C_3N_4 (JCPDS 00–87-1526) [34], suggesting their high purity. The mainly peaks at 13.0° and 27.5° were corresponding to the typical (0 0 1) and (0 0 2) crystal planes, respectively. [35] To further explore the structure of g-C_3N_4 sample, the FT-IR spectrum was measured. As shown in Fig. S2, several strong bands in the region of 1200–1650 cm^{-1} were found corresponding to the typical stretching modes of C–N heterocycles [36], and the broad peaks at around 3000–3480 cm^{-1} revealed the existence of incompletely condensed secondary and primary amines [37]. Additionally, the characteristic peak at 810 cm^{-1} was observed, which belonged to breathing mode of the triazine units [37]. XPS measurement was conducted to identify the chemical composition and bonding configuration of the as-fabricated products. In Fig. S3, the sample was mainly composed of C, N and O elements. The high-resolution XPS spectra were deconvoluted by Gaussian-Lorenzian analysis method. For C 1 s spectrum (Fig. 1a), three peaks at 284.7, 287.8 and 285.9 eV were observed, which were attributed to sp^2 C–C bonds, sp^2 hybridized carbon in N-containing aromatic ring (N–C=N) and the C−NH_2 species on the g-C_3N_4, respectively [38, 39]. In Fig. 1b, four fitted peaks were observed at around 398.1, 399.0, 400.3 and 403.9 eV, respectively. These peaks were regarded as the sp^2 hybridized nitrogen involved in triazine rings (C–N=C), the tertiary nitrogen N–$(C)_3$ groups, the free amino groups (C-N–H), and π-excitations, respectively [40]. The O 1 s peak (Fig. S4) was deconvoluted into two components at 531.9 and 533.4 eV, which were related to the adsorbed H_2O molecules and hydroxyl groups on the surface, respectively [38, 41].

The UV–Vis diffuse reflectance spectrum of g-C_3N_4 was illustrated in Fig. S5. The sample exhibited an absorption edge at about 470 nm, which indicated that g-C_3N_4 possessed response ability for visible light. Considering g-C_3N_4 to be an indirect semiconductor [42, 43], the band gap (E_g) was calculated to be about 2.75 eV.

3.2 Photocatalytic performance of RhB degradation

The photodegradation activities were evaluated under visible light irradiation ($\lambda > 420$ nm, Xe lamp light). In Fig. 2a, the self-degradation effect was ignored under visible light illumination. After 2 h visible-light irradiation, the efficiency for RhB degradation reached 92.0% over g-C_3N_4 sample, which was distantly higher than that of g-C_3N_4-B sample. Based on the N_2 adsorption measurement, the surface area of g-C_3N_4 reached 86 m^2/g, which was higher than that of g-C_3N_4-B (51 m^2/g). It meant that the double calcination promoted the surface area of photocatalyst. With decreasing pH value in the system, the RhB photodegradation rate increased gradually (Fig. 2b). In the acidic solution (pH 4.3), the efficiency of RhB degradation reached 99.1% after 15 min of illumination. Based on the above photocatalytic condition, the degradation efficiency still reached above 95% after the 8th cycling test (Fig. 2c). According to the XRD and XPS results of used sample (Fisg. S6 and S7), no obvious changes

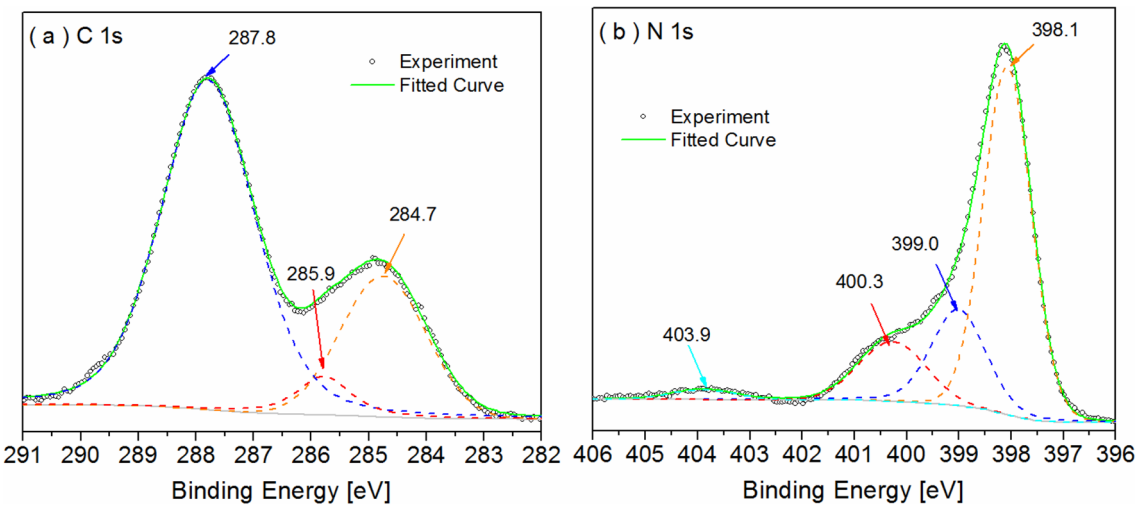

Fig. 1 XPS high-resolution spectra of **a** C 1 s and **b** N 1 s of the g-C_3N_4 sample

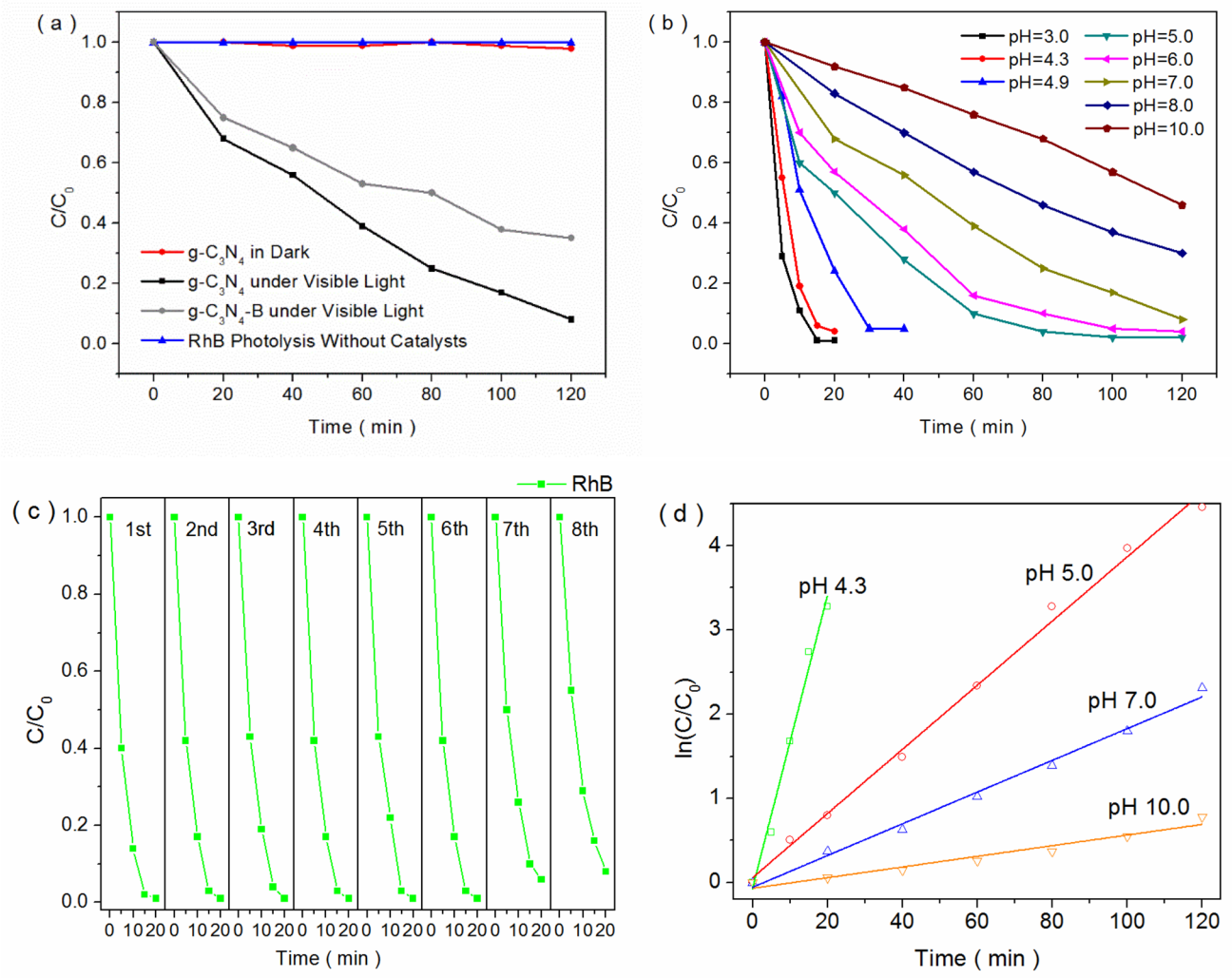

Fig. 2 Photocatalytic activity of RhB degradation over g-C_3N_4 using Xe lamp light(**a** blank test at pH 7.0, **b** catalytic system with different pH values, **c** cycling test at pH 4.3) and first-order kinetics plots for RhB photodegradation by g-C_3N_4 photocatalysts with different solution **d**

of the crystal structure and chemical state on the surface were discovered. In order to quantitatively understand the reaction kinetics of the RhB degradation, the photocatalytic process of RhB degradation followed the pseudo-first order kinetics model in our experimental condition (Fig. 2d) [23]. According to the apparent first-order linear transform, the pseudo-first order rate constant k was calculated and listed in Table S1. The result indicated a rather good correlation to the pseudo-first-order reaction kinetics ($R > 0.99$). The degradation rate decreased obviously with the increase of the pH values, and the rate constant k value in acidic system (pH 4.3) was about 8.6 times as much as that in neutral system (pH 7.0). It was implied that the hydrogen ion was a crucial factor in the photocatalytic degradation. Several existence forms of RhB molecules were observed in different solutions [44], and existence of RhB existed in a zwitterionic form in this study (pH 4 ~ 10). Considering the zero proton condition (ZPC) point of g-C_3N_4 (Fig. S8), the g-C_3N_4 sample showed superior adsorption ability toward RhB molecules in the solution with a high pH value (> 7.32) [45]. In addition, the adsorption process of the g-C_3N_4 material toward RhB was characterized by the Langmuir adsorption isotherm model (Fig. S9). The adsorption ability for RhB molecules in the solution of pH 10.0 reached 30.30 μmol/g. However, the excessive RhB molecules on the g-C_3N_4 surface inhibited the formation of oxygen radicals, which decreased the photodegradation efficiency. Hence, there was no certain correlation between the increase of photocatalytic performance and RhB adsorption ability over g-C_3N_4 photocatalyst.

The photocatalytic performance in acidic system (pH 4.3) was measured under natural sunlight and the results were shown in Fig. 3. After 30 min of sunlight illumination, the efficiency of RhB degradation reached about 95%. It was

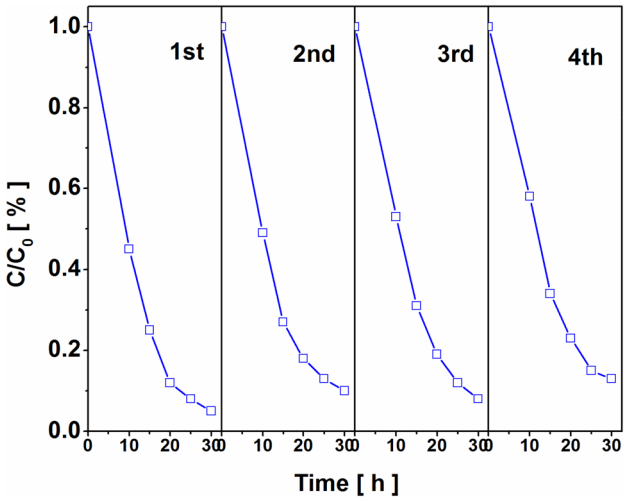

Fig. 3 Photocatalytic activity of RhB degradation over g-C_3N_4 in acidic system under sunlight

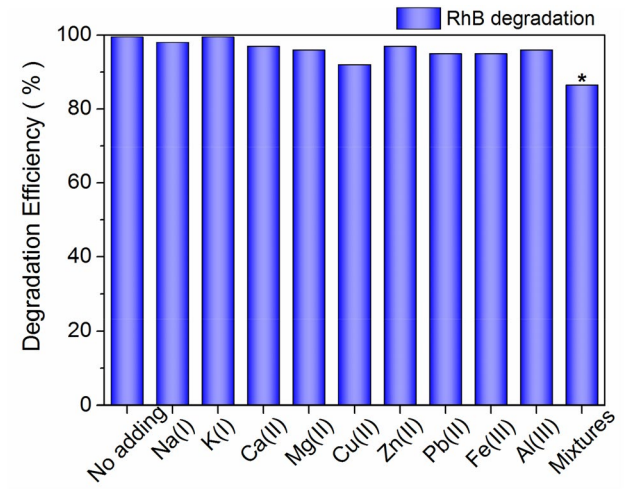

Fig. 4 Photocatalytic activity of RhB degradation over g-C_3N_4 in acidic solution (pH < 4.0) after 20 min irradiation(300 W Xe light) with different added metal-ion (0.05 mol/L). (*Added K(I), Na(I), Ca(II), Fe(III), Mg(II), Al(III), Zn(II) and Pb(II) after 30 min of sunlight irradiation)

notable that the photocatalytic activity still maintained above 85% in the 4th cycling under sunlight.

The influence of variety anions in real water system on the photocatalytic activity was not ignored. The degradation activities with multiple additional cations were measured. As shown in Fig. 4, the photocatalytic performance of RhB degradation in acidic system never decreased with cation disturbance. It was notable that the degradation efficiency reached 85% after natural sunlight irradiation in acidic solution containing mixed cations. Hence, the acidic system plays a positive effect on photocatalytic activity for RhB degradation over g-C_3N_4 material.

3.3 Photocatalytic process of RhB degradation

Figure 5 displayed the light absorption spectra of catalytic system during RhB degradation. The solution absorbance at pH values of 4.3 and 7.0 all decreased rapidly. The shift of the absorbance peak was observed at acidic system (pH 4.3) only if the decomposition was nearly completed (inset of Fig. 5a). Yet, a distinct shift (about 50 nm) occurred at pH 7.0 (inset of Fig. 5b). It implied that the hydrion in solution influenced the RhB degradation rate and decomposition process

To further investigate the process of RhB degradation, HPLC measurements were carried out, and the results were presented in Fig. 6. It was noted that other peaks, except for RhB molecule, were detected before irradiation both at pH 4.3 and pH 7.0, indicating that a small portion of RhB was degraded. After visible light irradiation (Xe lamp light), the signal intensity of RhB molecule remarkably declined with prolonging irradiation time. However, four new peaks appeared, which were on behalf of *N*-de-ethylated intermediates. The intensities of additional peaks were enhanced and then diminished gradually, which indicated the decomposition of dye structure. Considering the results of ESI-TIC/MS measurement (Figs. S10 and S11), the peaks of a (t_R 11.397 min), b (t_R 8.568 min), c (t_R 6.552 min), d (t_R 5.074 min) and e (t_R 4.076 min) were assigned to RhB, *N*,*N*,*N*'-tri-ethylated rhodamine (DER), *N*,*N*-di-ethylated rhodamine (DR), *N*-ethylated rhodamine (ER) and Rhodamine (R), respectively. Based on the above analysis, the depletion of the RhB absorbance was ascribed to the destruction of the conjugated structure. The hypsochromic shift of the absorbance peak position was due to the formation of a series of *N*-de-ethylated intermediates in a stepwise manner [21]. Therefore, during photodegradation process, RhB de-ethylation brought the wavelength change of its major absorption peak to move toward the blue region, which ranged from 552 nm (RhB) to 539 nm (DER), 522 nm (DR), 510 nm (ER) and 498 nm (R), respectively. According to the RhB degradation process in acidic system, it was found that the de-ethylation of RhB molecule was competitive with its cleavage [46, 47]. However, due to the distinct position shift of the absorbed peak in Fig. 5, the de-ethylation process played a main effect on the RhB degradation in neutral system.

Based on the LC/MS spectra (Fig. S12), two chromophore cleavage intermediates, including *N*-(2,4-dihydroxycyclohexa-2,5-dien-1-ylidene)-*N*-ethylethanaminium ($m/z = 182.1176$) and 4-(ethylamino) benzene-1,3-diol ($m/z = 153.0790$), were identified after 5 min of irradiation in acidic system, while these intermediates were not

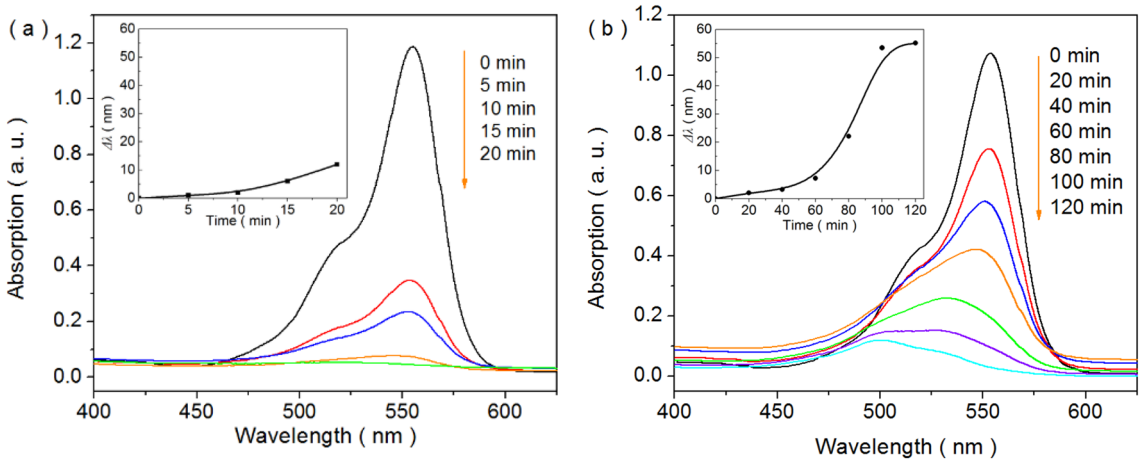

Fig. 5 Absorption spectra for RhB degradation in different systems (**a** pH 4.3 and **b** pH 7.0, the inset images: the changes of the maximum absorption wavelength)

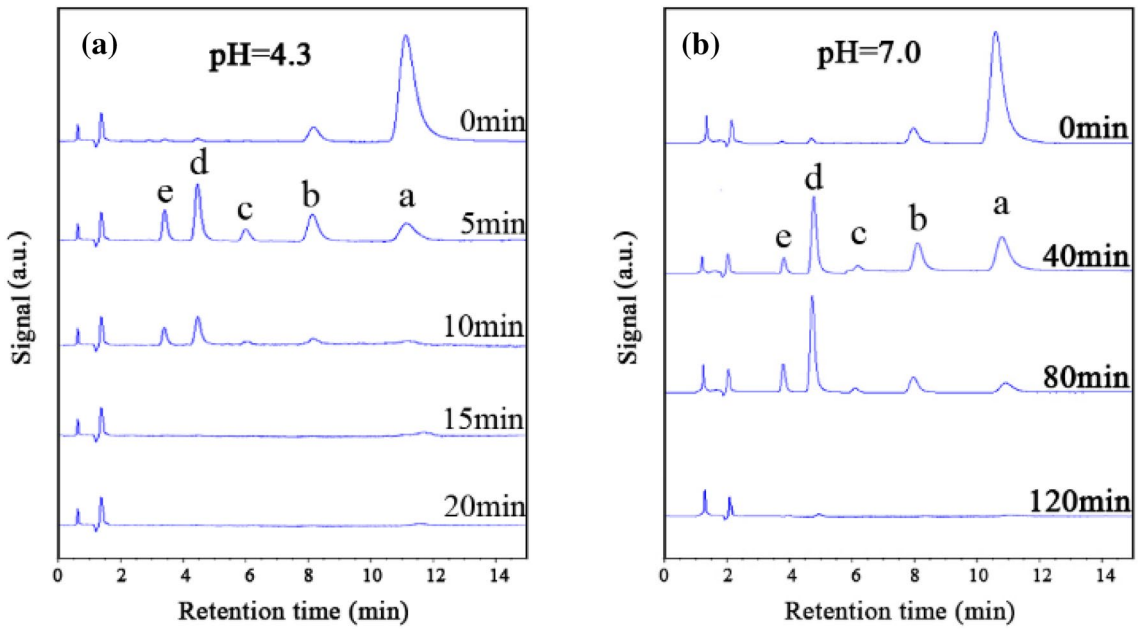

Fig. 6 HPLC spectra of RhB at different time of irradiation at pH 4.3 (**a**) and pH 7 (**b**)

detected in neutral solution. The results indicated that the de-ethylation process and chromophore cleavage happened simultaneously in the solution of pH 4.3, which enhanced the degradation efficiency. Combined with the results of reactive species, a large number of •OH in acidic system was beneficial to hydroxylation on chromophore and then lead to its cleavage. Besides, some other intermediates, such as organic acids, alkanol, ester and amine, were also identified by GC/MS and listed in Table S2. The benzene rings and 2,6-di-tert-butylphenol were produced from chromophoric cleavage in initial stages. Other detected intermediates were mostly chain compounds, which were derived from the cleavage of the xanthene ring in RhB molecule and *N*-de-ethylated intermediate structure by deethylation, hydroxylation and carboxylation [48]. These products were further oxidized to tetradecanoic acid, palmitic acid, stearic acid, 2,2-dihydroxyethyl palmitate, 2,3-dihydroxypropyl stearate, ethanamine, propan-1-amine, carbonic acid and propane-1,2,3-triol, which were further mineralized into CO_2, H_2O and NO_3^- [49]. On the basis of MS result (Fig. S12), the fragmentation pathway was proposed during photodegradation process.

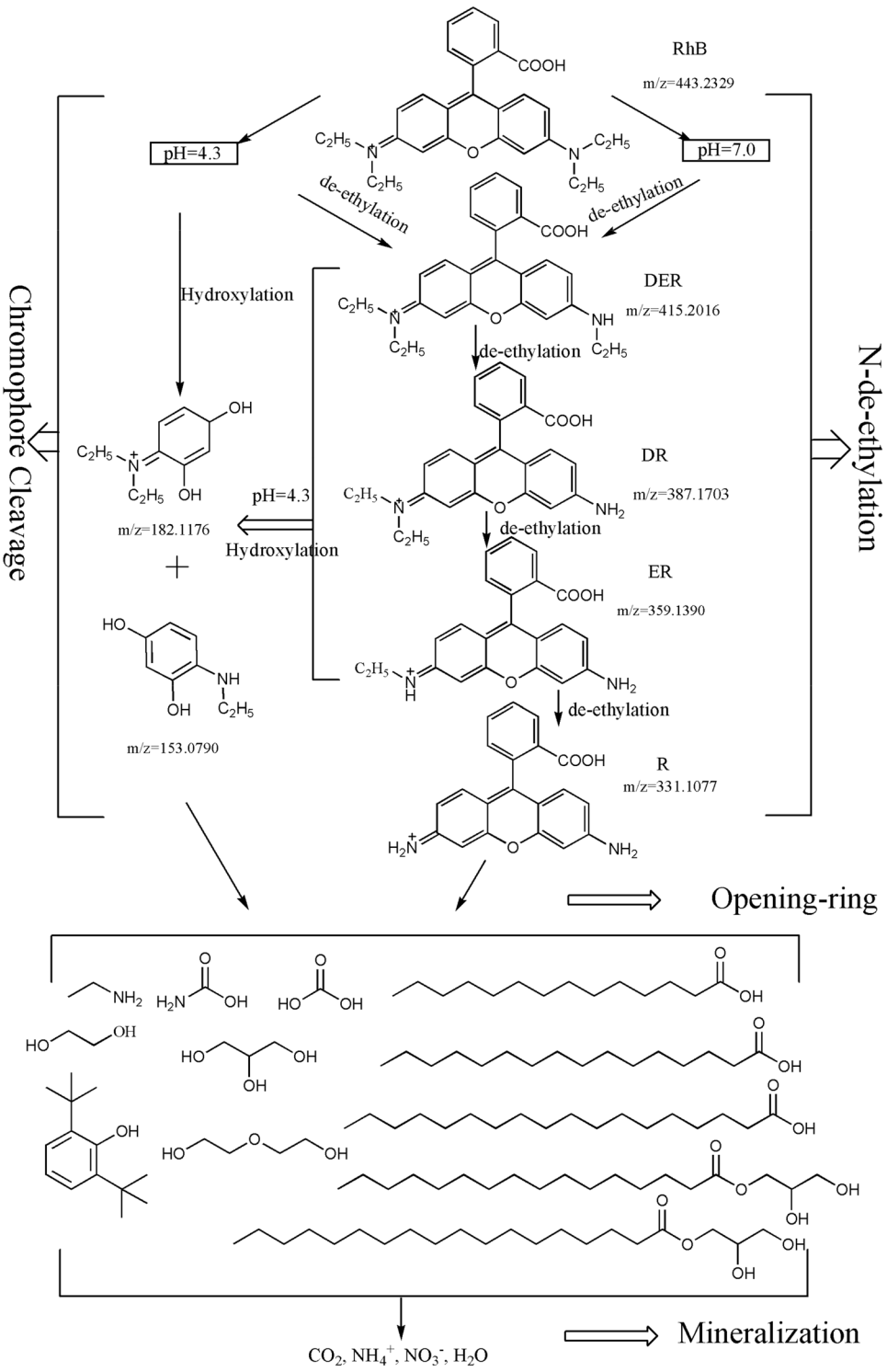

Scheme 1. Schematic diagram for RhB degradation over g-C_3N_4 photocatalysts

As shown in Scheme 1, the RhB molecule was degraded by the hydroxylation and de-ethylation process in the acidic solution (pH 4.3). For the neutral solution (pH 7.0), RhB molecule was decomposed by only de-ethylation reaction, and the degradation intermediates were further resolved into small molecules by deoxygenation and hydroxylation. The hydroxylation process in the acidic system promoted the photocatalytic efficiency of RhB degradation.

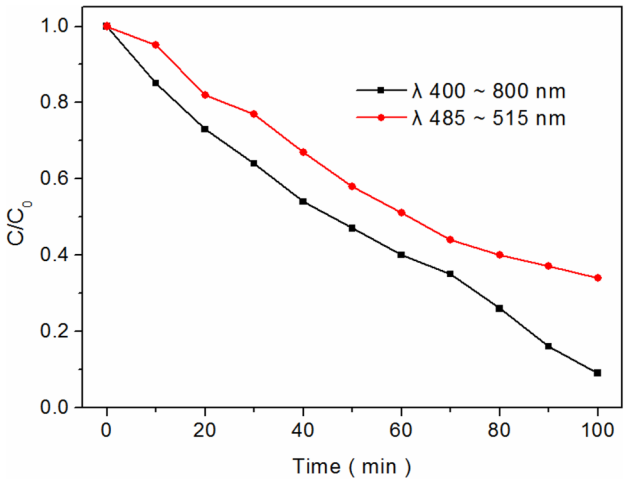

Fig. 7 Photocatalytic activity of RhB degradation over g-C_3N_4 under different light wavelength ranges with the same light intensity

3.4 Photocatalytic mechanism of RhB degradation

Photocatalytic mechanism is an important factor to further enhance the degradation efficiency. The photosensitization effect and direct electron–hole oxidation are vital for the photocatalysis of dye degradation. Since the as-prepared g-C_3N_4 only responded to the light energy with smaller wavelength ($\lambda < 460$ nm), a single wavelength filter of 500 nm was adopted to eliminate the photo-absorption of g-C_3N_4, exploring the photosensitization driven. As shown in Fig. 7, the degradation efficiency of RhB under 485 ~ 515 nm light irradiation still presented a slight decrease. Therefore, the degradation process was driven by RhB excitation.

Figure 8 displayed the effect of different scavengers on the photodegradation activities. In the case of neutral system (Fig. 8a, b), the degradation efficiency decreased markedly with excess addition of KI. It was indicated that the h_{VB}^+ and/or •OH species were important in the process of RhB

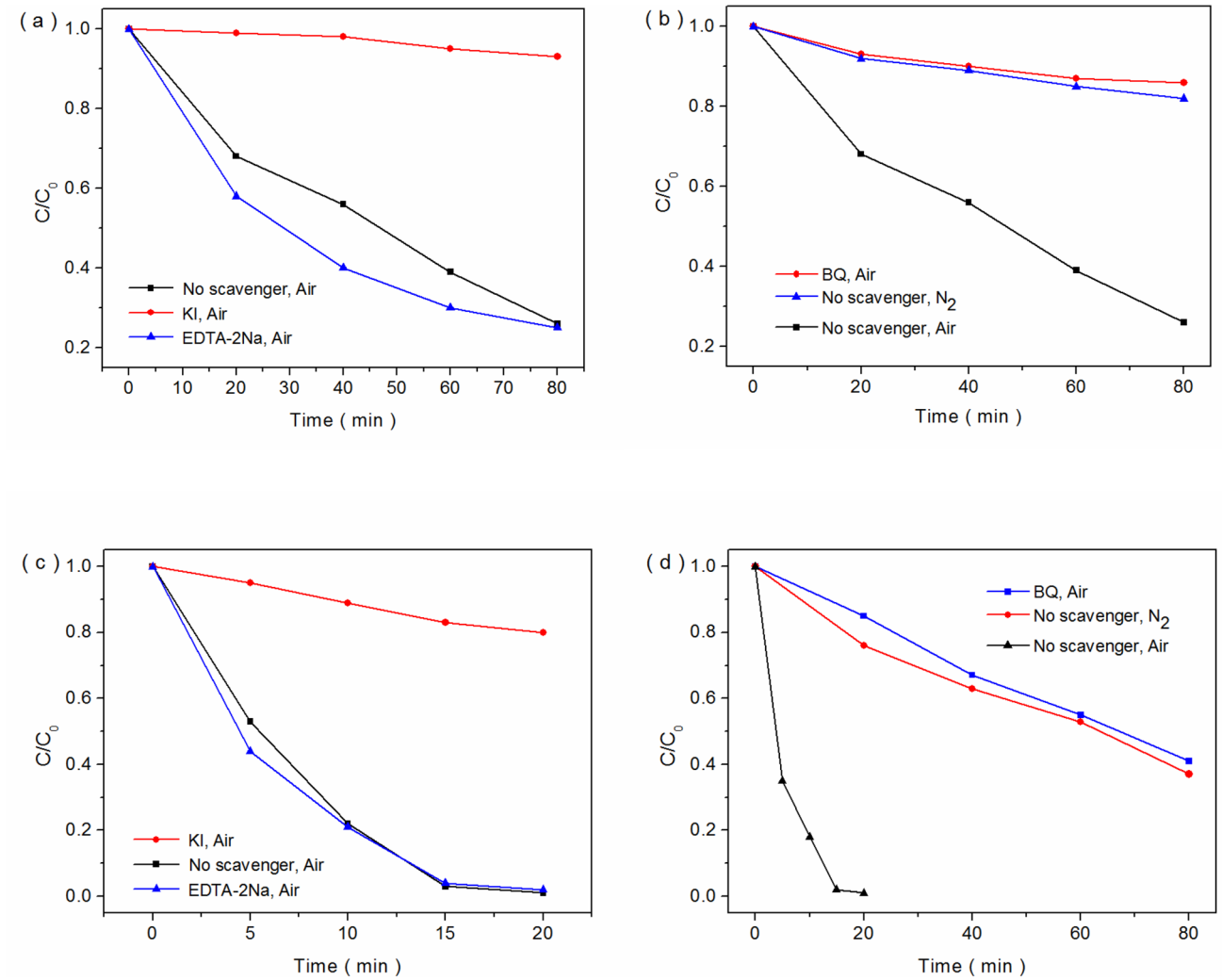

Fig. 8 Photocatalytic activity of RhB degradation over g-C_3N_4 in different solutions with pH 7.0 (**a**, **b**) and 4.3 (**c**, **d**)

oxidation. However, the addition of EDTA-2Na, as the scavenger of h_{VB}^{+}, did not distinctly inhibit the photocatalytic activity of RhB degradation. Furthermore, the addition of BQ suppressed the RhB degradation, which implied that $O_2^{-}\bullet$ was also the reactive specie in the degradation process. When the pH value of the solution was controlled to 4.7, similar results were achieved with addition of various scavengers (Fig. 8c, d). The above results suggested that •OH and $O_2^{-}\bullet$ radicals had significant effect on the process of RhB degradation.

It was known that the VB edge potential of g-C_3N_4 (+ 1.57 eV) was negative than the standard redox potential of •OH/OH^- (+ 2.38 eV vs. NHE) [50, 51]. Although •OH radicals were not formed by photogenerated holes in valence band of g-C_3N_4, RhB molecules were effectively decomposed, owing to the redox potentials of RhB and RhB* (0.95 and − 1.42 V vs. NHE). [22] Meanwhile, according to the calculated band gap (E_g) of g-C_3N_4, the CB edge potential was determined to be − 1.18 V (vs. NHE). The electrons from the excited RhB* were transferred to g-C_3N_4 providing a favorable driving force for the electron injection. In other words, the injected electrons caused the RhB photosensitization over g-C_3N_4 under 500 nm light irradiation. Additionally, the CB potential was more negative than the standard redox potential of $O_2/O_2^{-}\bullet$ (− 0.33 V vs NHE) [46]. A large quantity of $O_2^{-}\bullet$ species were produced from dissolved oxygen by the electrons in CB of g-C_3N_4. It was notable that $O_2^{-}\bullet$ radicals were apt to react with protons to form various active oxidizing species including the peroxy radical (HOO•) and hydrogen peroxide (H_2O_2), especially in acidic system. Therefore, the increasing content of hydrion promoted the photocatalytic performance of RhB degradation.

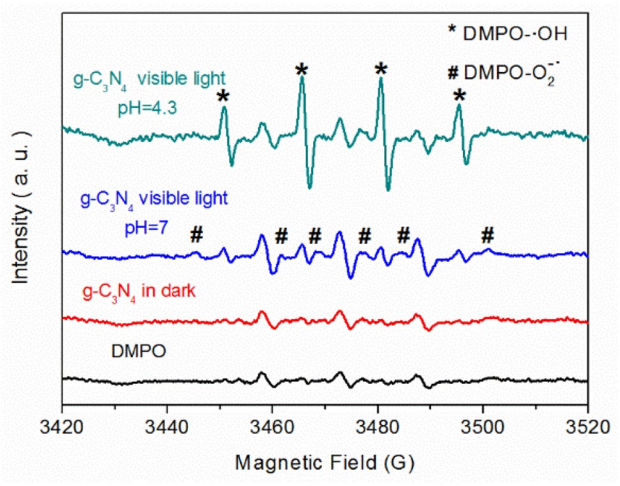

Fig. 9 ESR spectra for the DMPO-containing aqueous suspensions of g-C_3N_4 in solutions with different pH values after 10 min of visible light irradiation

ESR characterization was employed to further investigate the effect of •OH and $O_2^{-}\bullet$, and the results were shown in Fig. 9. DMPO-containing aqueous suspension of g-C_3N_4 displayed an obvious 1:2:2:1 quartet signal and a 1:1:1:1:1:1 sixfold signal after irradiation (Xe lamp light) which were the characteristics of DMPO-OH• and DMPO-$O_2^{-}\bullet$ [52, 53], respectively. It was indicated that OH• and $O_2^{-}\bullet$ were formed under irradiation.

In the acidic system (pH 4.3), the characteristic peaks of DMPO-OH• were observed, while the peaks assigned to DMPO-$O_2^{-}\bullet$ nearly disappeared. It was possible that abundant protons in the acidic system reacted smoothly with $O_2^{-}\bullet$ to generate a series of species including HOO• and •OH, [54] as shown in Eq. (1)–(4). Therefore, a large quantity of •OH was produced, and •OH radicals became the main active specie in acidic system (pH 4.3). Based on the band gap structures of g-C_3N_4 and RhB, combining the effects of scavengers and ESR analysis, the possible mechanism was proposed for the photodegradation of RhB over g-C_3N_4 in solutions with different pH values as follows:

$$O_2 + e \rightarrow O_2^{-}\bullet \quad (1)$$

$$O_2^{-}\bullet + H^+ \rightarrow HOO\bullet \quad (2)$$

$$2\,HOO\bullet \rightarrow O_2 + H_2O_2 \quad (3)$$

$$H_2O_2 + O_2^{-}\bullet \rightarrow OH^- + \bullet OH + O_2 \quad (4)$$

$$g - C_3N_4 + h\nu(\lambda > 400\ \text{nm}) \rightarrow e_{CB}^{-} + h_{VB}^{+}\left(g - C_3N_4\right) \quad (5)$$

$$RhB + h\nu(\lambda > 400\ \text{nm}) \rightarrow RhB^{*+} + e^{-}(RhB) \quad (6)$$

$$e^{-}(RhB) \rightarrow e_{CB}^{-}\left(g - C_3N_4\right) \quad (7)$$

$$e_{CB}^{-} + O_2 \rightarrow g - C_3N_4 + O_2^{-}\bullet \quad (8)$$

$$pH = 7,\ RhB^{*+}/RhB + \bullet OH/O_2^{-}\bullet/h_{VB}^{+} \rightarrow \text{degradation products} \quad (9)$$

$$pH \leq 4.3,\ O_2^{-}\bullet + H^+ \rightarrow HOO\bullet \quad (10)$$

$$2\,HOO\bullet + O_2^{-}\bullet \rightarrow OH^- + \bullet OH + 2\,O_2 \quad (11)$$

$$RhB^{*+}/RhB + \bullet OH/h_{VB}^{+} \rightarrow \text{degradation products} \quad (12)$$

4 Conclusions

In general, hydrion played a key role for photocatalytic RhB degradation over g-C_3N_4. The photocatalytic activity of g-C_3N_4 was increased gradually with decreasing pH values of catalytic solution, and the efficiency of RhB degradation reached nearly 95.0% within 20 min after 8 cycles in acidic solution (pH < 4.3). ·OH was induced by the reaction between hydrion and O_2^{-}· radical, and the RhB degradation occurred simultaneously via the successive deethylation of four ethyl groups and the direct degradation of the chromophoric system. Various oxidizing species and intermediates in the above two degradation processes were discovered by ESR, GC/MS and LC/MS measurements. In addition, the photosensitization efficiently promoted the photocatalytic activity. The investigation of RhB degradation system could establish a foundation for deeply understanding the degradation process of organic dyes.

Supplementary Information The online version contains supplementary material available at https://doi.org/10.1007/s43630-021-00019-9.

Acknowledgements This work was supported by the financial supports of National Natural Science Foundation of China (No. 51802082), Natural Science Foundation of Henan Province (212300410221), Program for Science & Technology Innovation Talents in Universities of Henan Province (No. 21HATIT016), Key Scientific and Technological Project of Henan Province (212102210473), Key Scientific Research Project of Henan Provincial Education Department (21A430030) and "Climbing" Project of Henan Institute of Science and Technology (No. 2018CG04).

Author contributions WS: Conceptualization, investigation, formal analysis, writing-review and editing, software. W-XF: Investigation, formal analysis, data curation. J-CW: Conceptualization, funding acquisition, formal analysis, writing-review and editing. XQ: Investigation, formal analysis. BW: Investigation, formal analysis. XG: Conceptualization, data curation, writing-review and editing.

Compliance with ethical standards

Conflict of interest The authors declare that they have no competing financial interests.

References

1. Huang, Q., Ye, Z., & Xiao, X. (2015). Recent progress in photocathodes for hydrogen evolution. *Journal of Materials Chemistry A, 3,* 15824–15837.
2. Tu, W., Zhou, Y., & Zou, Z. (2014). Photocatalytic conversion of CO_2 into renewable hydrocarbon fuels: state-of-the-art accomplishment, challenges, and prospects. *Advanced Materials, 26,* 4607–4626.
3. Wang, T., Luo, Z., Li, C., & Gong, J. (2014). Controllable fabrication of nanostructured materials for photoelectrochemical water splitting via atomic layer deposition. *Chemical Society Reviews, 43,* 7469–7484.
4. Chen, D., Zhang, X., & Lee, A. F. (2015). Synthetic strategies to nanostructured photocatalysts for CO_2 reduction to solar fuels and chemicals. *Journal of Materials Chemistry A, 3,* 14487–14516.
5. Li, X., Yu, J., Low, J., Fang, Y., Xiao, J., & Chen, X. (2015). Engineering heterogeneous semiconductors for solar water splitting. *Journal of Materials Chemistry A, 3,* 2485–2534.
6. Wang, Y., Zhang, F., Yang, M., Wang, Z., Ren, Y., Cui, J., et al. (2019). Synthesis of porous MoS_2/CdSe/TiO_2 photoanodes for photoelectrochemical water splitting. *Microporous and Mesoporous Materials, 284,* 403–409.
7. X. Xiao, S. Tu, M. Lu, H. Zhong, C. Zheng, X. Zuo & J. Nan, Discussion on the reaction mechanism of the photocatalytic degradation of organic contaminants from a viewpoint of semiconductor photo-induced electrocatalysis, *Applied Catalysis B:*, 2016, **198**, 124–132.
8. Liang, R., Jing, F., Shen, L., Qin, N., & Wu, L. (2015). MIL-53(Fe) as a highly efficient bifunctional photocatalyst for the simultaneous reduction of Cr(VI) and oxidation of dyes. *Journal of Hazardous Materials, 287,* 364–372.
9. W. Lu, T. Xu, Y. Wang, H. Hu, N. Li, X. Jiang and W. Chen, Synergistic photocatalytic properties and mechanism of g-C_3N_4 coupled with zinc phthalocyanine catalyst under visible light irradiation, *Applied Catalysis B:*, 2016, **180**, 20–28.
10. Park, H., Kim, H.-I., Moon, G.-H., & Choi, W. (2016). Photoinduced charge transfer processes in solar photocatalysis based on modified TiO_2. *Energy & Environmental Science, 9,* 411–433.
11. Qiu, P., Yao, J., Chen, H., Jiang, F., & Xie, X. (2016). Enhanced visible-light photocatalytic decomposition of 2,4-dichlorophenoxyacetic acid over $ZnIn_2S_4$/g-C_3N_4 photocatalyst. *Journal of Hazardous Materials, 317,* 158–168.
12. Willkomm, J., Orchard, K. L., Reynal, A., Pastor, E., Durrant, J. R., & Reisner, E. (2016). Dye-sensitised semiconductors modified with molecular catalysts for light-driven H_2 production. *Chemical Society Reviews, 45,* 9–23.
13. Reddy, P. A. K., Reddy, P. V. L., Kwon, E., Kim, K.-H., Akter, T., & Kalagara, S. (2016). Recent advances in photocatalytic treatment of pollutants in aqueous media. *Environment International, 91,* 94–103.
14. Zhang, W., Jia, B., Wang, Q., & Dionysiou, D. (2015). Visible-light sensitization of TiO_2 photocatalysts via wet chemical N-doping for the degradation of dissolved organic compounds in wastewater treatment: a review. *Journal of Nanoparticle Research, 17,* 221.
15. Liu, S., Sun, H., Ang, H. M., Tade, M. O., & Wang, S. (2016). Integrated oxygen-doping and dye sensitization of graphitic carbon nitride for enhanced visible light photodegradation. *Journal of Colloid and Interface Science, 476,* 193–199.
16. Gong, X., & Teoh, W. Y. (2015). Modulating charge transport in semiconductor photocatalysts by spatial deposition of reduced graphene oxide and platinum. *Journal of Catalysis, 332,* 101–111.
17. Hamdy, M. S., Saputera, W. H., Groenen, E. J., & Mul, G. (2014). A novel TiO_2 composite for photocatalytic wastewater treatment. *Journal of Catalysis, 310,* 75–83.
18. Tokode, R. Prabhu, L. A. Lawton and P. K. J. Robertson, Effect of controlled periodic-based illumination on the photonic efficiency of photocatalytic degradation of methyl orange, *Journal of Catalysis*, 2012, **290**, 138–142.
19. Qian, Y., Wang, L., Du, J., Yang, H., Li, M., Wang, Y., & Kang, D. J. (2021). A high catalytic activity photocatalysts based on porous metal sulfides/TiO_2 heterostructures. *Advanced Materials Interfaces, 7,* 2001627.
20. L. Yang, Y. Xiao, S. Liu, Y. Li, Q. Cai, S. Luo and G. Zeng, Photocatalytic reduction of Cr(VI) on WO_3 doped long TiO_2 nanotube arrays in the presence of citric acid, *Applied Catalysis B*, 2010, **94**, 142–149.

21. Cui, Y., Ding, Z., Liu, P., Antonietti, M., Fu, X., & Wang, X. (2012). Metal-free activation of H_2O_2 by g-C_3N_4 under visible light irradiation for the degradation of organic pollutants. *Physical Chemistry Chemical Physics, 14,* 1455–1462.
22. J. Hu, W. Fan, W. Ye, C. Huang and X. Qiu, Insights into the photosensitivity activity of BiOCl under visible light irradiation, *Applied Catalysis B*, 2014, **158–159**, 182–189.
23. Merka, V. Yarovyi, D. W. Bahnemann and M. Wark, pH-Control of the photocatalytic degradation mechanism of rhodamine B over $Pb_3Nb_4O_{13}$, *Journal of Physical Chemistry C*, 2011, **115**, 8014–8023.
24. Fang, S., Lv, K., Li, Q., Ye, H., Du, D., & Li, M. (2015). Effect of acid on the photocatalytic degradation of rhodamine B over g-C_3N_4. *Applied Surface Science, 358,* 336–342.
25. Yue, X., Liu, Z., Zhang, Q., Li, X., Hao, F., Wei, J., & Guo, W. (2015). Oxidative degradation of rhodamine B in aqueous solution using Fe/PANI nanoparticles in the presence of AQS serving as an electron shuttle. *Desalination and Water Treatment, 57,* 15190–15199.
26. Wei, Z., Spinney, R., Ke, R., Yang, Z., & Xiao, R. (2016). Effect of pH on the sonochemical degradation of organic pollutants. *Environmental Chemistry Letters, 14,* 163–182.
27. Guo, Z., Zhang, J., & Liu, H. (2016). Ultra-high rhodamine B adsorption capacities from an aqueous solution by activated carbon derived from Phragmites australis doped with organic acid by phosphoric acid activation. *RSC Advances, 6,* 40818–40827.
28. Tian, J., Olajuyin, A. M., Mu, T., Yang, M., & Xing, J. (2016). Efficient degradation of rhodamine B using modified graphite felt gas diffusion electrode by electro-fenton process. *Environmental Science and Pollution Research, 23,* 11574–11583.
29. Hu, X., Ji, H., Chang, F., & Luo, Y. (2014). Simultaneous photocatalytic Cr(VI) reduction and 2,4,6-TCP oxidation over g-C_3N_4 under visible light irradiation. *Catalysis Today, 224,* 34–40.
30. Wu, H., Qian, Y., Cui, J., Chai, Q., Du, J., Zhang, L., et al. (2019). Enhanced interfacial charge transfer and separation rate based on sub 10 nm MoS_2 nanoflakes in situ grown on graphitic-C_3N_4. *Advanced Materials Interfaces, 6,* 1900554.
31. Ye, S., Wang, R., Wu, M.-Z., & Yuan, Y.-P. (2015). A review on g-C_3N_4 for photocatalytic water splitting and CO_2 reduction. *Applied Surface Science, 358,* 15–27.
32. Zhu, J., Xiao, P., Li, H., & Carabineiro, S. A. (2014). Graphitic carbon nitride: synthesis, properties, and applications in catalysis. *ACS Applied Materials & Interfaces, 6,* 16449–16465.
33. Sui, Y., Liu, J., Zhang, Y., Tian, X., & Chen, W. (2013). Dispersed conductive polymer nanoparticles on graphitic carbon nitride for enhanced solar-driven hydrogen evolution from pure water. *Nanoscale, 5,* 9150–9155.
34. Wang, Y., Shi, R., Lin, J., & Zhu, Y. (2011). Enhancement of photocurrent and photocatalytic activity of ZnO hybridized with graphite-like C_3N_4. *Energy & Environmental Science, 4,* 2922–2929.
35. Wang, X., Maeda, K., Thomas, A., Takanabe, K., Xin, G., Carlsson, J. M., et al. (2009). A metal-free polymeric photocatalyst for hydrogen production from water under visible light. *Nature Materials, 8,* 76–80.
36. Li, X., Zhang, J., Shen, L., Ma, Y., Lei, W., Cui, Q., & Zou, G. (2008). Preparation and characterization of graphitic carbon nitride through pyrolysis of melamine. *Applied Physics A: Materials Science & Processing, 94,* 387–392.
37. Niu, P., Liu, G., & Cheng, H.-M. (2012). Nitrogen vacancy-promoted photocatalytic activity of graphitic carbon nitride. *Journal of Physical Chemistry C, 116,* 11013–11018.
38. Q. Lin, L. Li, S. Liang, M. Liu, J. Bi and L. Wu, Efficient synthesis of monolayer carbon nitride 2D nanosheet with tunable concentration and enhanced visible-light photocatalytic activities, *Applied Catalysis B*, 2015, **163**, 135–142.
39. Li, J., Shen, B., Hong, Z., Lin, B., Gao, B., & Chen, Y. (2012). A facile approach to synthesize novel oxygen-doped g-C_3N_4 with superior visible-light photoreactivity. *Chemical Communications, 48,* 12017–12019.
40. Yu, J., Wang, K., Xiao, W., & Cheng, B. (2014). Photocatalytic reduction of CO_2 into hydrocarbon solar fuels over g-C_3N_4-Pt nanocomposite photocatalysts. *Physical Chemistry Chemical Physics: PCCP, 16,* 11492–11501.
41. Dong, G., Ai, Z., & Zhang, L. (2014). Efficient anoxic pollutant removal with oxygen functionalized graphitic carbon nitride under visible light. *RSC Advances., 4,* 5553–5560.
42. G. Dong, Y. Zhang, Q. Pan and J. Qiu, A fantastic graphitic carbon nitride (g-C_3N_4) material: Electronic structure, photocatalytic and photoelectronic properties, *Journal of Photochemistry and Photobiology C*, 2014, **20**, 33–50.
43. Wang, J. C., Yao, H. C., Fan, Z. Y., Zhang, L., Wang, J. S., Zang, S. Q., & Li, Z. J. (2016). Indirect Z-scheme BiOI/g-C_3N_4 photocatalysts with enhanced photoreduction CO_2 activity under visible light irradiation. *ACS Applied Materials & Interfaces, 8,* 3765–3775.
44. Watarai, H., & Funaki, F. (1996). Total internal reflection fluorescence measurements of protonation equilibria of rhodamine B and octadecylrhodamine B at a toluene/water interface. *Langmuir, 12,* 6717–6720.
45. Hashemzadeh, F., Gaffarinejad, A., & Rahimi, R. (2015). Porous p-NiO/n-Nb_2O_5 nanocomposites prepared by an EISA route with enhanced photocatalytic activity in simultaneous Cr(VI) reduction and methyl orange decolorization under visible light irradiation. *Journal of Hazardous Materials, 286,* 64–74.
46. Li, W., Li, D., Meng, S., Chen, W., Fu, X., & Shao, Y. (2011). Novel approach to enhance photosensitized degradation of rhodamine B under visible light irradiation by the $Zn_xCd_{1-x}S/TiO_2$ nanocomposites. *Environmental Science and Technology, 45,* 2987–2993.
47. L. Hu, F. Yang, W. Lu, Y. Hao and H. Yuan, Heterogeneous activation of oxone with CoMg/SBA-15 for the degradation of dye Rhodamine B in aqueous solution, *Applied Catalysis B*, 2013, **134–135**, 7–18.
48. Soltani, T., & Entezari, M. H. (2013). Sono-synthesis of bismuth ferrite nanoparticles with high photocatalytic activity in degradation of Rhodamine B under solar light irradiation. *Chemical Engineering Journal, 223,* 145–154.
49. Natarajan, T. S., Thomas, M., Natarajan, K., Bajaj, H. C., & Tayade, R. J. (2011). Study on UV-LED/TiO_2 process for degradation of Rhodamine B dye. *Chemical Engineering Journal, 169,* 126–134.
50. Yan, S. C., Lv, S. B., Li, Z. S., & Zou, Z. G. (2010). Organic-inorganic composite photocatalyst of g-C_3N_4 and TaON with improved visible light photocatalytic activities. *Dalton Transactions, 39,* 1488–1491.
51. L. Ge, C. Han and J. Liu, Novel visible light-induced g-C_3N_4/Bi_2WO_6 composite photocatalysts for efficient degradation of methyl orange, *Applied Catalysis B*, 2011, **108–109**, 100–107.
52. Yan, S. C., Li, Z. S., & Zou, Z. G. (2009). Photodegradation performance of g-C_3N_4 fabricated by directly heating melamine. *Langmuir, 25,* 10397–10401.
53. Dong, G., & Zhang, L. (2013). Synthesis and enhanced Cr(VI) photoreduction property of formate anion containing graphitic carbon nitride. *Journal of Physical Chemistry C, 117,* 4062–4068.
54. C. Tan, G. Zhu, M. Hojamberdiev, K. Okada, J. Liang, X. Luo, P. Liu and Y. Liu, Co_3O_4 nanoparticles-loaded BiOCl nanoplates with the dominant {001} facets: efficient photodegradation of organic dyes under visible light, *Applied Catalysis B*, 2014, **152–153**, 425–436.